RISK ANALYSIS OF EX-SPOOL 16″ MOL: AN INSIGHT OF MACHINE LEARNING AND EXPERIMENTAL RESULT

The paper reports the development of a Risk-Based Inspection (RBI)-Machine Learning perspective. The Optical Emission Spectrometry (OES), Tensile and Hardness Test, Scanning Electron Microscope (SEM), Energy Dispersive X-Ray Spectroscopy (EDS), Sulfate Reducing Bacteria Check, and X-Ray Diffraction (XRD) was used to analyze the root cause of the pipeline's failure. Corrosion attack shows at the cross-section microstructure based on SEM results. Carbon, Manganese, Phosphorous, and sulfur's chemical composition is dramatically lower than the standard API 5L Grade X42. Siderite and hematite dominate the composition of the corroded area as a result of CO_2 dissolving in water. In contrast, hematite is generated due to the pipe and outdoor atmosphere reaction. Severe local wall thinning of the sand abrasion causes the degradation of the material's mechanical properties and increases the corrosion rate. This result amplifies by the development of Machine Learning (ML) of Pearson Multicollinear Matrix and Supervised ML (Random Forest, Support Vector Machine, and Linear Regression) to estimate the corrosion degradation of the material. The source of datasets provided by ILI inspection includes the calculated PoF Remaining Useful Life (RuL) as input data, while Probability of Failure (PoF) prediction serves as output data. The Random Forest shows superior predictions of 92.18 %, with the lowest validation loss of 0.0316. The modeling result confirms the experimental outcome. This work demonstrates the implementation strategy to reduce the analysis time, minimize human bias, and serve as a reliable reference tool and guideline to maintain the integrity of the subsea pipelines

Keywords: Root-cause-analysis, Wall thinning, Sand Abrasion, Pearson Multicollinear Matrix, Supervised Machine Learning

Taufik Aditiyawarman
Corresponding author
Master of Science, Doctoral Degree Student*
E-mail: taufik.aditiyawarman@pertamina.com
Johny Wahyuadi Soedarsono
Doctor of Engineering, Professor*
Agus Paul Setiawan Kaban
Master of Engineering, Doctoral Degree Student**
Rini Riastuti
Doctor of Engineering, Senior Lecturer**
Haryo Rahmadani
Bachelor of Engineering, Surface Facility Engineer**
Mohammad Pribadi
Master of Science, Senior Engineer**
Rizal Tresna Ramdhani
Bachelor of Science, Bachelor of Engineering,
Master of Engineering, Senior Engineer**
Sidhi Aribowo
Master of Science, Senior Engineer**
Suryadi
Master of Engineering, Senior Researcher
Center for Materials Processing and Failure Analysis (CMPFA)
Manufacturing Research Center
Faculty of Engineering***
*Department of Metallurgy and Material Engineering***
**Prof Johny Wahyuadi Laboratory
Department of Metallurgical and Materials Engineering***
***Universitas Indonesia
Kampus Baru UI Depok, Jawa Barat, Indonesia, 16424

1. Introduction

Pipelines are critical tools to deliver the fluids of hydrocarbon as a source of energy. It is not limited, but most pipelines in modern society are even used to transport flammable, explosive, and corrosive fluids [1]. In an aggressive medium with minimum corrosion mitigation and risk-based assessment, the material tends to fail and causes severe financial consequences. Recently, a few publications have reported the risk of material related to oil pipelines [2–4]; however, the studies have not covered the influence between the root cause analysis (RCA) and the calculated risk to mitigate the reoccurrence of failure.

The sole RCA is insufficient to reveal why the material failed without collecting and analyzing all risk possibilities related to the properties and environment of the pipelines. Furthermore, the mitigation plan may suffer from inadequacy correlated to assessing the corresponding risk. The incomplete gap between the two is critical to reassuring that the mitigation plan has been delivered properly to prevent the failure from reoccurrence. This study offers an alternative approach to unveil the benefit of gaining an in-depth

primary cause of material's failure to re-measure the risk. Therefore, it is necessary to study the connection between the RCA and risk evaluation from given pipelines to guarantee the deliverable of oil and gas meets the demands of industry and society.

Recently, risk-based inspection (RBI) risk assessment has extended to the utilization of Machine Learning (ML). Authors of [5–7] argue that the risk assessments are subjective and often dissimilar to the actual condition of assessed pipelines. The model of RBI remains to suffer from why the impact of corrosion varies despite the uniformity of treatment, such as the addition of biocide, pigging, and cathodic protection. By considering the limitation, the engineer would not correctly deduce the appropriate pipeline integrity mitigation plan (PIM) due to a lack of data management handling and data processing about the actual condition of pipelines. In addition, it would impose a higher financial issue due to higher operational costs and unsuitable recommendations for pipeline integrity. ML models can reduce higher dimensional data and calculate the risk based on the relationship between risk input and output parameters. It aims to predict the actual condition of pipelines without discharging the need for the actual inspection. Hence, combining RCA and RBI based on ML can be implemented into daily operational practice where it resolves the primary issue of the conventional RCA and RBI.

2. Literature review and problem statement

The RCA model is essential to identifying the failure of metals and has become a critical tool in modern industrial development. Without RCA, the business impact of material loss consumes the company's time and finances, especially in the oil and gas (O&G) industry. Some mitigation strategies have been implemented, including using a green corrosion inhibitor [8–11], failure analysis (FA) [12], and Risk-Based Inspection (RBI) based on AI [6]. Amongst the strategies, the blending implementation of FA and AI is critical to preventing uncertainty-induced risk. A recent publication reports that AI implementation's advantage is reducing the processing data analysis time [5]. In addition, this advent of information technology minimizes the human subjectivity in measuring the risk. The above knowledge has become the primary reason for the suitability implementation between the FA and AI.

The validation of the preceding arguments lies in recognizing the source of failure, including implementing several laboratory assessments and utilizing Machine Learning (ML). Previous studies by [13] show the sole role of fault analysis relates to the diagnosis technique. The research uses gradient boosting to improve the identification of the fault in twin study cases in the chemical process industry. However, the study reports its inability to identify some true root causes of the flaw. The other research by [14] argues that the matrix materials examination detects the corrosion product and suggests the possible pitting corrosion appearance. Despite its achievement, the model of RCA remains to suffer in predicting the pairwise related corrosion parameter quickly.

However, the above studies neglect the essential information of the pipeline's actual condition and the utilization of provided data to suggest valuable maintenance recommendations. This work discusses the recent advent of technology in sensors of Inline Inspection (ILI), which operates the intelligence pigging to supply the defect of pipelines' information to help identify the RCA analysis. ILI is a widespread technique used to help evaluate the condition of unprotected pipelines. Several types of intelligence pig are magnetic flux leakage (MFL), ultrasonic testing (UT), and electromagnetic acoustic transducer (EMAT) [1]. According to the author [15], ILI is utilized to monitor the health condition of the pipelines and ensure the inspection schedule and activities to minimize the risk and cost of unavoidable corrosion. The tool can identify defect detection, predict the defect's growth, and serve as a risk management system.

The paper[16] shows the RCA's role in controlling internal corrosion due to impure gasses (CH_4, CO_2, H_2S) and Microbiological Induced Corrosion (MIC) bacteria. The paper discusses the significance of palm oil corrosion inhibitors in reducing the effect of the above factor. But there were unresolved issues related to measuring the pipeline's wall thinning in considering its time in service and its remaining development. The principal reason for these inadequacies lies in the measure of the actual condition of pipelines. This objective makes the relevant analysis impractical and has an inherent bias in objectively assessing the recommendation.

On the other hand, the work of [17] elaborates the role of ILI and Internal Corrosion Direct Assessment (ICDA) in distinguishing between the piggable and non-piggable pipelines. The work presents adequate information on the corrosion threat and implements the National Association of Corrosion Engineers (NACE) standards. Although the generated assessment is valid in unveiling the location of internal corrosion, the study demonstrates the limitation of risk assessment and analysis. The research of [18] compares the previous survey to reveal the exact failure location of a pipeline through the implementation of RBI. The work tackles the research limitation by selection and optimization of direct assessment of the high-risk pipelines. The paper mainly discusses the various corrosion growth without considering the difficulties associated with the risk heterogeneity from the effect of contaminant CO_2 gas.

In addition, the paper of [19] argues the role of anti-corrosion protection against the threat of CO_2 gas and their development. The conducted research uses the field assessment to identify the most aggressive internal corrosion condition and analyze the normative documentation to record the findings. Due to the unprecedented situation recently, the higher frequency of field inspection is costly and imposes tremendous effort to maintain the integrity of pipelines.

In contrast, the other researcher [20] introduces a novel technique to remove the effect of oil sands deposition due to their aggressive abrasion on the inner side of pipelines. The report highlights the ranking system of the corroded material based on the corrosion degradation assessment and eventually reduces the cost of the inspection. However, the missing part of the research is the discussion related to the growth of microbiologically induced corrosion (MIC). The MIC has been considered responsible for the rapid increase of MIC due to the formation of H_2S and $FeCO_3$. A similar hypothesis was proposed to impose pipelines' rapid deterioration through biofilm formation on the coupon's surface.

A way to overcome these difficulties can be resolved using the combination of RCA and intensive application of ML. On one side, the RCA is an attractive method for many researchers and practitioners. A recent study by [21]

equips the research by developing the ultrasonic sensor to internally overcome the obstacles of crack visualization and generate the anomaly's historical datasets. At the same time, ML retains its validity in gathering and processing the ILI data to provide comprehensive studies of the failed materials. The work of [22] reviews several methods of collecting the potential datasets from the field inspection results and their historical data.

On the other hand, the risk execution based on the recorded data may not be sufficient to assess the risk without conducting a direct inspection such as ILI is also critical. The author of [23] describes the benefit of ILI in significantly impacting the assessment of the pipeline integrity management program. The works model that ILI is a promising tool to study the severity level of pipelines and detect possible threats corresponding to unresolved pipeline issues. The challenge in using the ILI database shows the processing time required to handle and process the massive data. It includes the possible duplication and irrelevant datasets from several parameters of measurement. The most prominent method to overcome these difficulties is optimizing ML performance in which the entire data of ILI is treated as features. At the same time, the calculated risk of PoF is considered labels.

All this allows to assert that it is expedient to conduct a study on devoted are to mapping the relationship between the root cause factors and the severity assessment to ensure the proper implementation of maintenance of pipelines.

3. The aim and objectives of the study

The study aims to offer a new perspective to address the scientific issue of RCA related to the practice of RBI using ML as a primary tool in measuring the risk of the failed pipeline.

To achieve this aims, the following objectives are accomplished:

– to analyze the failed material, including its chemical composition and mechanical properties;

– to identify the classification of corrosion compounds using metallography, SEM, EDX, and XRD characterization;

– to study the effect of bacterial activity in increasing the threat of corrosion due to the richness of organic acids;

– model the failure material using the Supervised ML by implementing the confusion matrix and SVM, RF, and LR algorithms to minimize human subjectivity and bias.

4. Materials and Methods

4. 1. Object of research

The paper aims to improve the model of RCA and offers a new era for utilizing the experimental result in predicting the probability of failure (PoF). The work further harnesses the laboratory data and uses the ILI data to give a valid recommendation of the likelihood of material to fail. Up to the author's knowledge, the proposed research methodology would impair the existing RCA technique and project the PoF's score aiming to reconstruct the maintenance plan. This work highlights the use of fundamental ILI-generated data such as fatigue, embrittlement, wall thinning, and degradation of the internal coating and collects the data to assess the risk. All mentioned factor becomes a significant part of the consideration to seek the root cause of the API 5L Grade X42 as a means to transport oil and calculate the risk.

The risk matrix projects the risk profile where the multiplication of Probability of Failure (PoF) and Consequence of Failure (CoF) corresponds to its severity level. However, there are various standards to determine the failure of structural reliability, such as DNV, 2010a [24], 2010b [25]. The calculated PoF of API 581 of Remaining Useful Life (RuL) is implemented in this paper to enhance the RCA from the same material. The motivation for using PoFRuL is to indicate the pipelines' actual condition and incorporate the failure prediction.

4. 2. Materials

The as-received specimen of the subsea pipeline has a specification of API-5L-X52 PSL2, as illustrated in Table 1.

Table 1

The detailed specification of material

Parameters	Data
Outer diameter (inch)	14
Wall Thickness (inch)	0.5
Length (km)	21.3
Design pressure (psig)	500

The characterization process was performed based on the above specification.

4. 3. Methods

4. 3. 1. Chemical composition characterization

Sample material of ex-spool 16″ was subjected to a chemical composition test. One small piece of the material was prepared and sectioned for a flat surface before conducting Optical Emission Spectroscopy (OES). The test follows the standard of ASTM A751 and E415 using WAS Lab Foundry-Master Oxford Instrument. The flat specimen was burned using a spark to create optical emission due to electron excitation in the metal specimen. The detector then analyzed the optical emission for each spectrum in the optical emission. Each element has a spectrum pattern, and the spectrum's intensity corresponds with the concentration of the component in the material. The examination intends to obtain the percentage composition of Carbon (C), Manganese (Mn), Phosphorous (P), Sulfur (S), and Iron (Fe) which impacted the failure of the material.

4. 3. 2. Visual Examination, Hardness, and Tensile Test

The pipe was cut into two sections in the longitudinal direction. For each specimen, one set of specimen was prepared for the tensile test while the other was utilized for the hardness test. The visual examination was conducted to verify the color of the internal coating and the surface of the dent layer. The tensile specimen is tested under the ASTM E8 standard using Shimadzu Servopulser. The dog bone specimen was uniaxially tensioned using a tensile machine until the specimen gauge length had a fracture. The change of load and specimen extension were recorded to measure the stress and strain in the specimen. The examination's expected result identifies the dent location and the leakage direction.

Moreover, the hardness test was conducted on sample material using Rockwell Hardness Tester Machine. The sample preparation was similar to the previous method. The test was conducted under ASTM E18 using Rocky DR Rockwell. The flat specimen was indented using Rockwell B indenter, a hardened steel ball. The sample was first loaded with a

minor load of 10 kg to fix the indenter and then continued by loading with a significant load of 100 kg to give permanent indentation on the material surface.This examination intends to examine the dispersion of corrosion products on the surface of metals. This knowledge allows the engineer to predict the types of corrosion and their root cause.

4. 3. 3. Metallography Examination

The specimens were cut and prepared for metallographic examination. The preparation for metallographic examination includes mounting, grinding, polishing, and etching. The etching was conducted using Nital solution to reveal the microstructure and morphology. The specimen preparation was completed by ASTM E3 using Buehler Metaserv-250, and the observation of the specimen under the microscope was conducted per ASTM E407 using Olympus GX41 – Inverted Metallurgical Microscope. The etching technique revealed the microstructure, which controlled corrosion on a specific phase in the steel material. The work selected two test locations to examine the crack area specimen and their adjacent crack area.

4. 3. 4. SEM-EDX Characterization

A scanning electron microscope (SEM) test was conducted on the surface area of the sample material at the crack area to observe the feature of the surface area. The specimen observation using a scanning electron microscope was conducted using FEI Inspect F50. The microanalysis of the corrosion product was utilized using energy-dispersive X-ray spectroscopy (EDX) embedded with SEM. The scanning of the specimen in the SEM instrument was carried out using an electron beam. A microphotograph was generated using a secondary electron (SE) model to produce a topographical image. Further examination of the corrosion product was performed using the EDX method by utilizing the specimen's excitation. The detector measured the X-ray intensity and was proportional to the concentration of elements on the spot. Moreover, the test's expected result correlated to the corrosion product's structure.

4. 3. 5. X-ray Diffraction Characterization (XRD)

The analysis of corrosion products was conducted using the XRD (Philips PW 24 X-Ray Spectrometer). Moreover, the powder specimen of the corrosion product was exposed to an X-Ray to obtain the diffraction pattern. The result of diffraction was then analyzed using X'Pert High score software.

4. 3. 6. Bacterial activity sampling

The analysis of bacterial activity was inspected semi-quantitatively using the Sani-Check SRB. The seawater was taken from the inside of leakage pipelines and filtered from the debris precipitate upon pigging activity completion. The standard seawater solution was placed inside the conical flask at 250 mL and allowed one night to change the color. The series of 5 dilution solutions was prepared to ensure variation population growth of the bacteria. The depth of solution cloudinessequals the highest amount of bacteria to 10^6 colony/ml.

4. 3. 7. Machine Learning modeling and Pearson Multicollinear Matrix

As previously outlined, the ML shows its capability to measure the relationship between the ILI parameters and the PoF. The total dataset is 1451 instances. The source of data was generated from the ILI inspection of the inspected pipelines (Supplementary 1). Table 2 shows the input and output data to capture the ML model's use further.

Table 2

The detail of input and output data in the intelligent system

Input Data	Output Data
Distance of pipeline	
Length of pipeline	
The width of the wall thinning	
The thickness of the wall thinning	PoF Prediction
PoFRuL	
Corrosion rate	

Appendix 1 summarizes the ILI data, which covers the information in Table 2. Pearson Correlation Matrix implements to compute Pearson's correlation coefficient. The strong correlation coefficient was given beyond 0.5, while the lower value was removed as reported in the published work of[26]. In addition, this work was carried out using a standard computer with 120 GB SSD storage, RAM 8 GB, and Intel i5. The work used the open source of Phycharm Community Edition 2021.3 embedded with a Jupyter notebook. Also, the project used several libraries of *Pandas, Keras, NumPy, sklearn.ensemble, and sklearn.metrics.*

4. 3. 8. Logistic Regression (LR)

Based on the publication of [27], the correlation between the input and output datasets was measured using the function of logistic regression. It utilizes the probability of the datasets belonging to particular classes. Equation (1)shows the likelihood calculation as reported in [28]:

$$\left\{ \log it\left(p\right) = \log\left(\frac{p}{1-p}\right) = \alpha + \beta^T x \right\}. \tag{1}$$

In the above equation, p is the probability, α is the linear regression function, and β^T is the coefficient vector regression [22]. The predictive value of the corroded metal is in the binary numbers 0 (Not failed) and 1 (Failed). At the same time, logit(p) is considered a *Y*-axis that defines the prediction of a material's failure probability based on the input data. The selected parameters are «liblinear» solver and the «ovr» multi_class.

4. 3. 9. Random Forest

An ensemble classifier of Random Forest (RF) provides better performance than a single classifier. The RF compiles the decision trees' value that comprises the random input dataset to replace the initial dataset as cited in the previous work [29]. The utilization of an ensemble algorithm prevents training data overfitting and advantages the variation with fewer correlations between predicted and the error of prediction. The work of [26] elaborates a comprehensive discussion of RF.

4. 3. 10. Support Vector Machine (SVM)

The fundamental principle of SVM corresponds to separating a set of binary datasets located in feature space with maximum hyperplane to give optimum separation margin from two classes. In this study, the input data set is considered an element vector $X_i \in R^n$ (Table 1). The value of 0 and 1 correlates to the prediction of severe or non-severe condition

of the pipeline. Therefore, the equation (2) shows the calculation of the hyperplane that separates two classes [30],

$$\{f(x) = w^T \times \phi(x) + b = 0\}. \qquad (2)$$

In the above equation, w is the vector normal, b corresponds to bias, and $\phi(x)$ is the feature map to convert the input feature to a space of higher-dimensional space.

5. Result of research of RCA-RBI based Machine Learning

5. 1. Root cause analysis results

5. 1. 1. Chemical composition results

Table 3 shows the OES result of the pipe material's chemical composition. The material complies with the speciation referred to as API 5L Grade X42 PSL 1.

Table 3

Chemical Composition results

Sample Code	C(%)	Mn(%)	P(%)	S(%)	Fe(%)
Spool 16″	0.14	0.43	0.021	0.022	Bal.
API 5L Grade X42 PSL 1	0.28max	1.3max	0.03max	0.03max	Bal.

The material is considered mild carbon steel with a higher composition of Manganese (0.43 %) and Sulfur (0.022 %). In comparison, the Phosphorous is slightly lower than the rest of the elements (0.021 %), as depicted in Table 3.

5. 1. 2. Results of Visual Inspection, Hardness, and Tensile Tests

Upon the pipeline cutting, the subsea pipeline's visual inspection shows a dent in the sectional direction, as illustrated in Fig. 1.

Fig. 1 reports the source of the leakage at the 6 o'clock position and generally from the pipeline ID. In addition, a dent appears on the surface of the failed material (Fig. 2, a). The complete sectioning of the leak area reveals the peeled-off surface in the surrounding area, as illustrated in Fig. 2, b.

The result of the removal layers of the coating indicates the abrasive material intensively contacts and damages the coating surface. It is also essential to notice that the peeling of the layer shows in a right-hand side direction over the dent. Tables 4, 5 present the hardness and tensile test results to determine the ex-spool material's mechanical properties.

Table 4

The Hardness Test Result of Ex-Spool

Sample Code	Hardness
Spool 16"	80 HRB
API 5L Grade X42 PSL 1	NA

From the above information, the hardness of the specimen is 80 HRB. This value is in conjunction with the spool's high microstructural inhomogeneity. The result impacts how these properties correlate to the probability of failure and approximation of the remaining useful

life (RuL). Hence, proper investigation of the hardness test advantages the preparation and maintenance plan of the pipelines. Table 5 shows that the test result's tensile strength is lower than the minimum specified magnitude value under the design codes and standards.
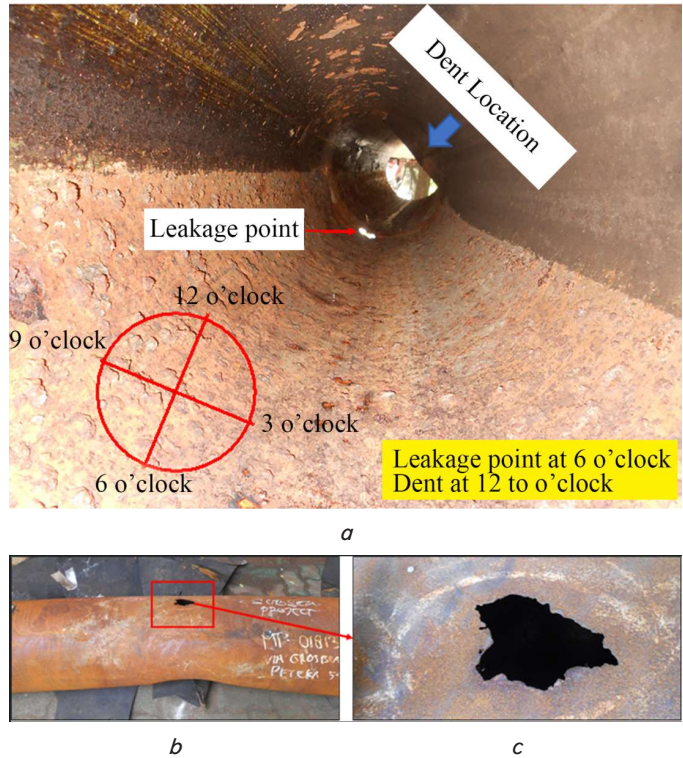

Fig. 1. The condition of: a — the clock position of pipelines; b — the opposite part of the dent

Fig. 2. The specimen of: a — peeled-off coating; b — suspected abrasive affected area

Tensile Test Result

Sample Code	Tensile Strength, MPa	Yield Strength, MPa	Elongation (%)
Ex-Spool 16" MOL	451	368	33
API 5L Grade X52 PSL-1	460 min	360 min	–

As a result, the failed sample shows an extension of 33 % elongation while the yield strength (368 MPa) is higher than the standard code. Hence, from the previous mechanical evaluation characterization, it can be concluded that the material has lost its ability to withstand load and is susceptible to failure (Table 5). This result demonstrates the complete alignment with the Hardness test and visual examination.

5. 2. Corrosion Product Analysis Results

The metallography, SEM, and EDX analysis of corrosion products show the actual condition on the surface of MS. Fig. 3, *a* shows the types of ex-spool specimen's ferrite and pearlite microstructure. The white grain represents the ferrite, while the dark grain is associated with the pearlite. In addition, there is no evidence to show the defect in the specimen's microstructure.

The results indicate that all micrographs exhibited CO_2 corrosion due to the $FeCO_3$ accumulation [31], which causes severe pitting corrosion to occur in and around the pearlite regions (Fig. 3, *b*). This phenomenon confirms the speed of the flow of erosive material to increase the rate of pitting corrosion along the direction of the pits of teardrop-shaped (Fig. 1, *a*).

A surface morphology study intends to understand the internal losses due to corrosion. Fig. 4, *a* shows the flowery structure of the scanned leakage area, and it corresponds to Fe_2O_3 or γ-FeOOH as a corrosion product. In addition, the presence of cotton balls correlated to the α-FeOOH (goethite).

Location 1 highlights the leakage of the pipeline at the exact location, while the adjacent inspected site is shown in location 2. Fig. 4 illustrates the crystal structure of iron oxides (cotton ball and flowery) and their irregular forms. The shallow cubic structure (Fig. 4, *b*) correlates to the presence of $Fe(CO_3)_3$. The above result is comparable to the research of [32]. The compound agrees with the outcome of EDX, shown in Table 6.

Based on Table 6, the amount of Fe and O dominates the number of other compounds. The above result confirms iron carbonate and iron oxide are exhibited in the leak location. The same table illustrates the presence of sulfur in both areas, in which location 1 shows a higher percentage of S than that of the second location. The common elements Fe, Si, C*l*, O, and S, proposed the microbial activity from the organic

The feature of corrosion products can be further studied by identifying their morphology using XRD. Fig. 5 illustrates the types of corrosion products.
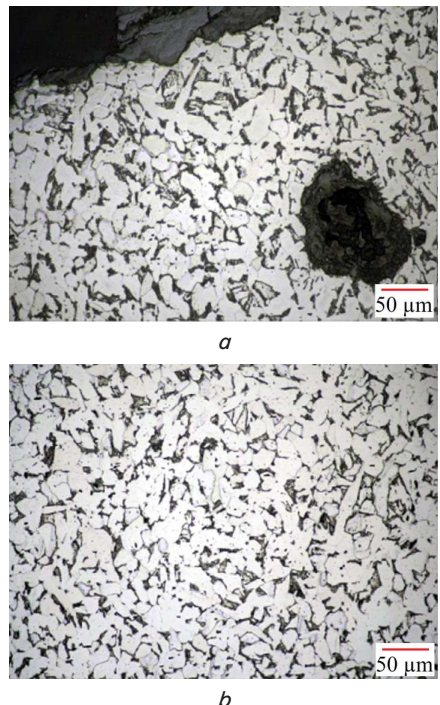

Fig. 3. The microstructure of: *a* — taken from the area far from the leakage; *b* — Microstructure of the cross-section Ex-spool 16″ MOL
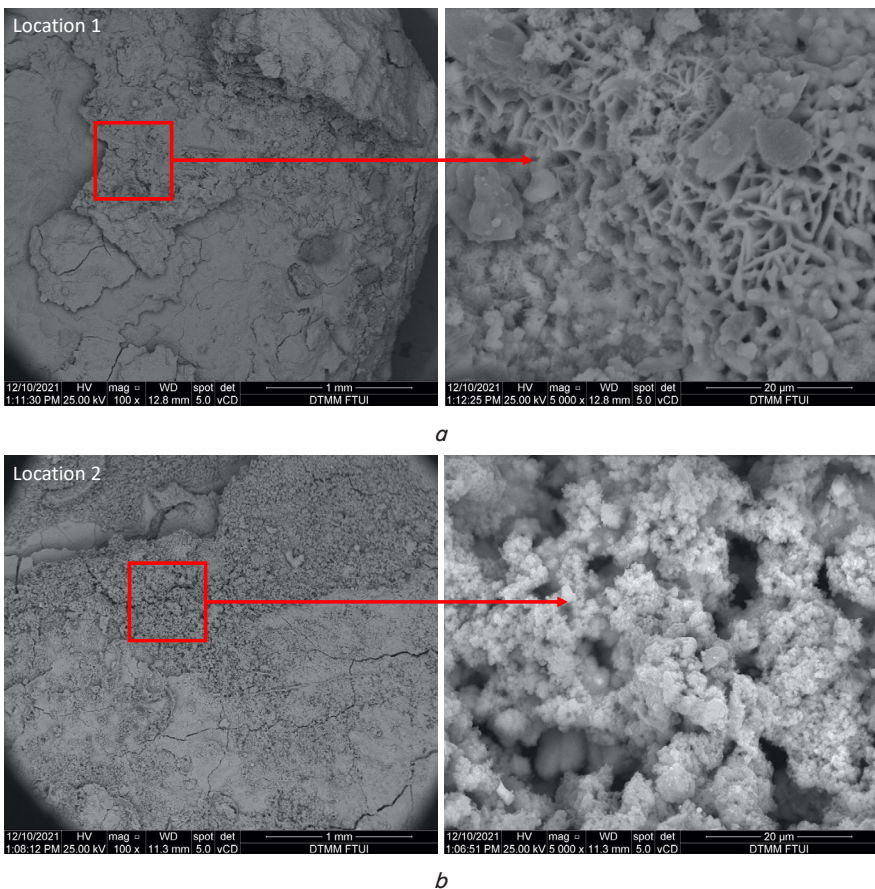

Fig. 4. The SEM image of the two inspected of *a* — Location 1; *b* — Location 2

Fig. 5 shows the collection of corrosion products from the internal pipeline. It comprises iron sulfate, iron carbonate, iron sulfide, and iron oxides. The appearance of troilite (FeS) formation is affected by the dissolved hydrogen sulfide gas (H_2S) in water. This compound agrees with the appearance of the Sulfur atom, as shown in Table 7. Moreover, the siderite formation is affected by dissolved carbon dioxide gas (CO_2) in water.

Table 6

The EDX Result of Two Locations

Element	Location 1 Wt(%)	Location 2 Wt(%)
Fe	61.77	63.44
O	26.28	29.98
Mn	1.17	0.84
Cl	4.13	2.50
S	1.36	0.79
Si	1.77	1.13

The XRD analysis shows the peak of $FeSO_4$, FeS, $FeCO_3$, Fe_3O_4, and Fe_2O_3 (Fig. 5). Siderite, magnetite, and hematite dominate deposited as the corrosion product detected on all rusted areas. However, the score of siderite 12 demonstrates that the CO_2 reacts with Fe and deposits on the surface of the metal. The formation of Fe_2O_3 and Fe_3O_4 results from aqueous corrosion and weathering of the pipe material during outdoor exposure.
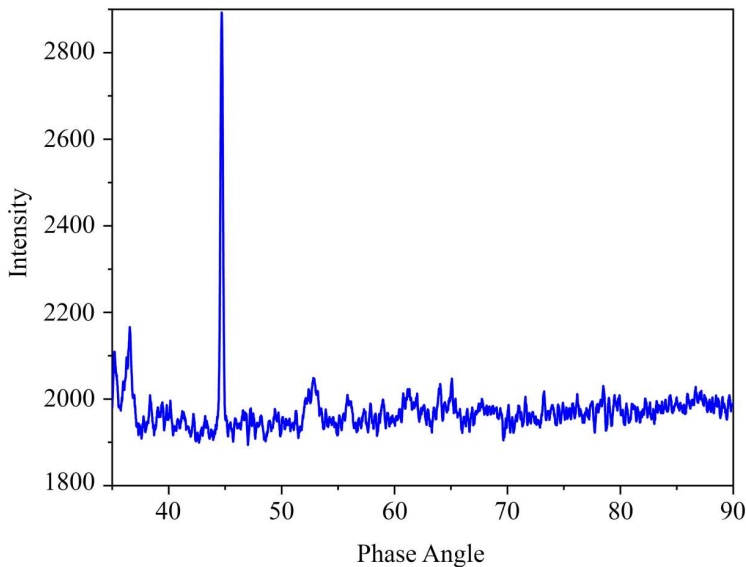

Fig. 5. The XRD Characterization of the Ex-spool specimen

Table 7

The corrosion products XRD analysis results from the area around the leakage.

Ref. Code	Score	Compound Name	Displacement (°2θ)	Chemical Formula
00-001-0703	4	Iron Sulfate	−0,293	$FeSO_4$
00-001-1247	3	Troilite	0,118	FeS
00-003-0746	12	Siderite	−0,014	$FeCO_3$
01-074-0748	8	Magnetite	−0,323	Fe_3O_4
01-085-0599	5	Hematite	−0,428	Fe_2O_3

5. 3. Bacterial activity result

Fig. 6 shows the bacterial monitoring result from January to December 2020 to assert the presence of sand deposition, and organic material increases the corrosion rate.
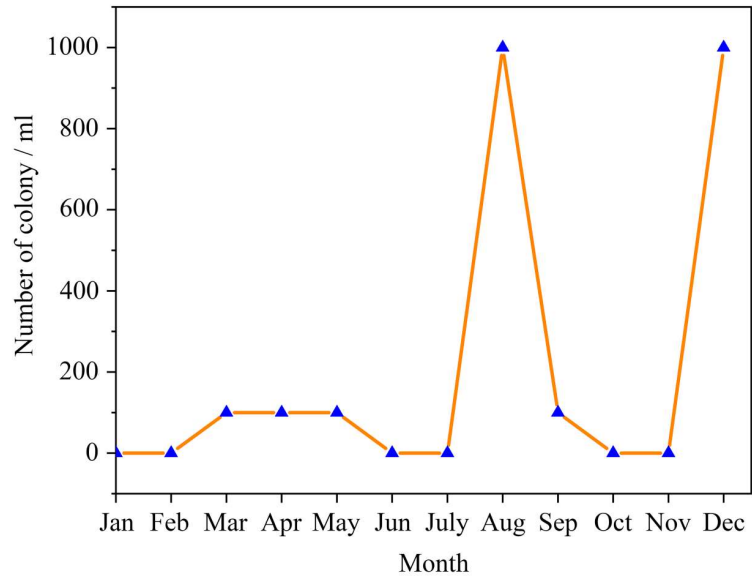

Fig. 6. The SRB monitoring result

As stated in the previous section, the microorganism activity increases the susceptibility to metallic corrosion. Sulfate-reducing bacteria (SRB) doubles the corrosion rate of carbon steel since it produces sulfides [33] and consumes hydrogen in cathodic reactions [30]. As shown in Fig. 6, the bacteria colonies rose dramatically in August and December, increasing the evolution of hydrogen gas and conductive FeS. These activities occur on the surface area of the bacteria's cell [34].

5. 4. Machine Learning studies result

This paper presents the selected features: log distance (the distance between the oil well and the inspected anomaly in the pipelines), length, width, and peak depth corresponding to the corrosion product, corrosion rate, PoFRuL, and PoF prediction. Fig. 7 shows the quality of the model, and according to the author [35], a pairwise score of less than 0.5 indicates irrelated pairwise.

In contrast, the more significant pairwise identification when the scores are more than 0.5 provides reliable inferences. The length and width of the pit corrosion identify to exhibit a low relationship with a score of 0.33. The relationship between the PoFRuL has a strong relationship (0.88) with PoF prediction. Moreover, the corrosion depth matches the PoFRuL as it has a score of 1, as depicted in Fig. 7. The PoF prediction and the pipeline distance showed no correlation as it has a low score of (−0.14). Also, there is a weak correlation between the width of siderite and the PoF prediction (0.064).

The primary tool implemented for identifying relevancy between the features and labels is Machine learning. Features (input data) are the corrosion-caused parameters. This model's label is the learning output attributed to the PoF prediction. The value determines the significance of

ML to forecast the failure of material while suggesting the inspection time upon the flaw of materials. It is essential to remember that PoF prediction may address the human bias and subjectivity in classifying any pipeline defect. Fig. 8 shows the performance of the ML models, Random Forest (RF) outperforms the Linear Regression (LR) and Support Vector Machine (SVM). The hyperparameter of modeling represents the optimum modeling condition in RF using the ILI datasets.

As summarized in Fig. 8, the RF provides the highest accuracy of 92.18 %, with the lowest validation loss of 0.031604, despite an intensive model evaluation required to confirm this hypothesis. Likewise, LR of 67.81 % provides the most insufficient accuracy with a validation loss of 0.031604.
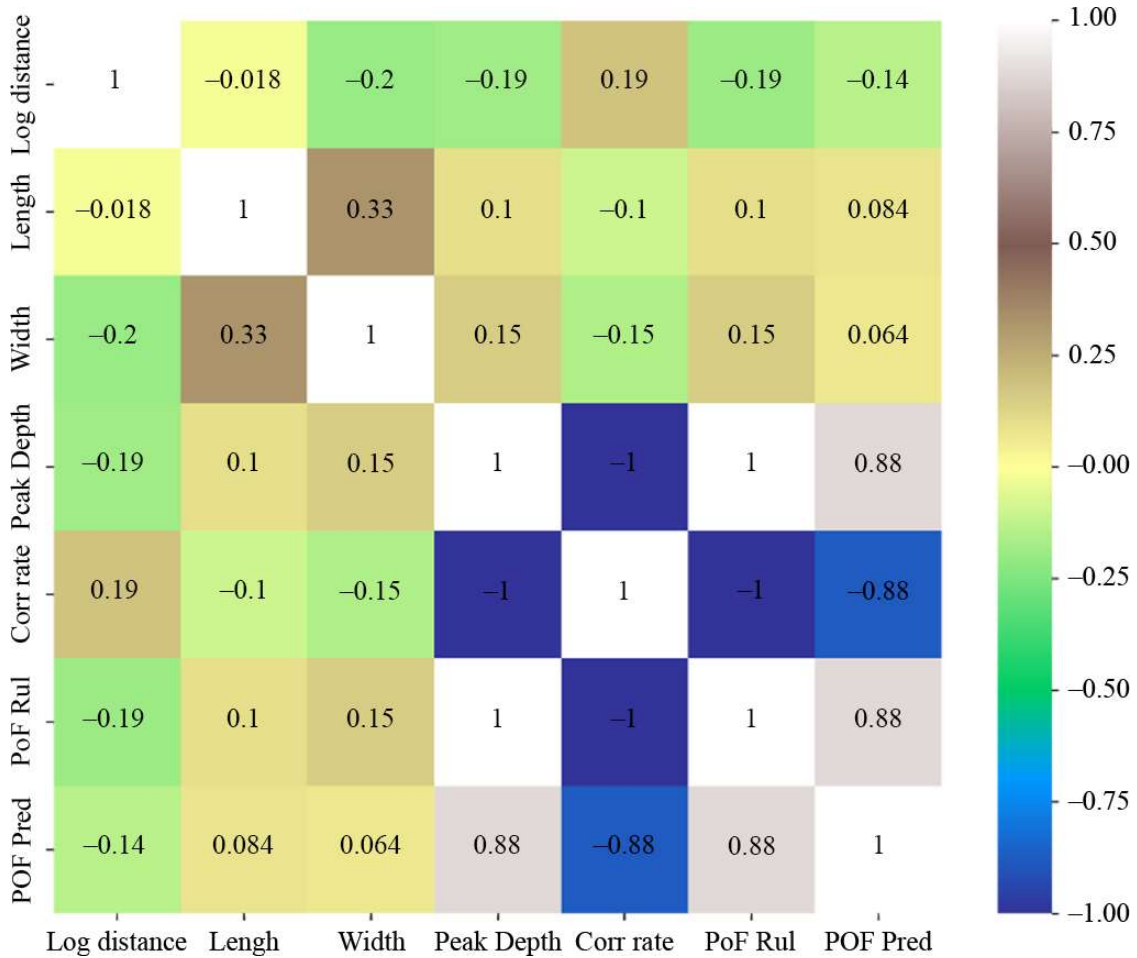

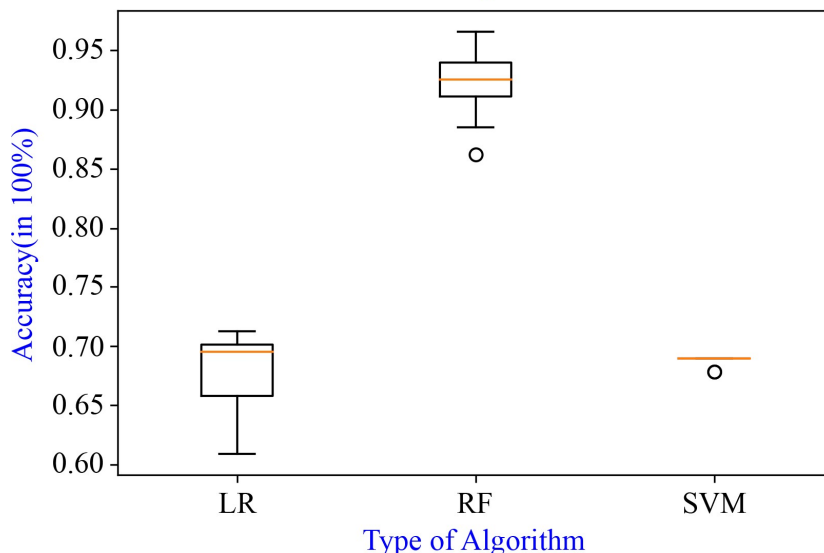
Fig. 7. The Pearson Multicollinear Matrix

Fig. 8. The comparative performance of ML

6. Discussion of RCA analysis and Risk Modelling

The amount of elements in the specimen corresponds with their fundamental chemistry composition to determine the corrosion resistance. Table 2 compares the elemental percentage between the ex-spool material with the standard API 5L composition. It can be seen that the smaller amount of element correlates to the dissolution of the element during the service. Also, the presence of manganese and sulfur increases the ability of the metal to adverse the effect of corrosion. The lower amount of manganese (5 %) suggests the ex-spool tends to rust, although it has a minor contribution to the overall material's degradation [36]. The study [37] shows that Mn remains an essential element in reducing the erosion velocity of sand through the solid strengthening of manganese.

The evolution of phosphorous (P) content after the material has been in service for several years reveals under specification (0.021 %) versus (0.03 %). The result lowers the hardness and corrosion resistance due to the damage to the amorphous structure in the interface of metal-metalloid alloys [38]. Furthermore, the content of sulfur (S) is 0.022 %, and it shows the role of S as a metal passivator to reduce the corrosion containing sulfur corrosion. A recent study [39] shows a similar result; however, the alloy remains susceptible to attack by corroded chloride ions since the ex-spool materials are submerged in seawater.

Fig. 9 illustrates the anomaly on the ex-spool material to showcase the pipe's dent, which is approximately 18 % inward and reduces the inner diameter at the dent location. The position shows that the corrosion mechanism after a certain period in service decreases the wall thickness of the inner surface of the pipelines. Moreover, it can also confirm the presence of teardrop-shaped pit corrosion resulting from elongating the fluid flow direction. The presence of a green internal coated surface exfoliated at the exact location proves that during the commissioning period, the engineer painted the inner layer of pipelines. It is also critical to note that the unpeeled coating shows many scratch lines oriented towards the lengthwise of the pipelines. No shallow pits nor channeling appeared, resulting in the leak in another location. It confirms that the leakage originated in the opposite area against the dented area. The leak progresses due to high fatigue life as the pipeline is submerged in seawater [22]. It increases the localized deformation levels on the inner pipe surface where it initiates the crack to grow.

Also, a dent in the pipeline caused inward deformation and reduced the pipeline's inner diameter while restricting the internal flow. Thus, as a consequence, localized turbulence and increased velocity can be expected to occur in this dent area. This turbulence and higher flow velocity might be detrimental to the internal pipe surface when combined with the fine sands, as shown by the presence of debris inside the pipeline (Fig. 9).

The result is comparable with the research conducted by [40] where the degradation of metal in the inner layer of the pipe resulting severe growth of wall thinning. Moreover, it can be seen from the illustration that the turbulence occurred at the inward dent protrusion. However, the observed lines on the remaining coating material prove an abrasion in the area around the dent whenever the pigging process is performed.

The combination of dent pipe, high velocity, and sand particles inside the pipe has created an abrasion effect on the internal pipe wall. This abrasion effect slowly removed the coating material and caused the corrosion attack on the pipe material (CS). The turbulence of sand particles was then collaborated to further release the corrosion products on the area where the coating was removed. It results from a severe wall thinning, leading to leakage. As previously highlighted, the corrosion product reveals the presence of iron carbonate with little iron sulfide [41].
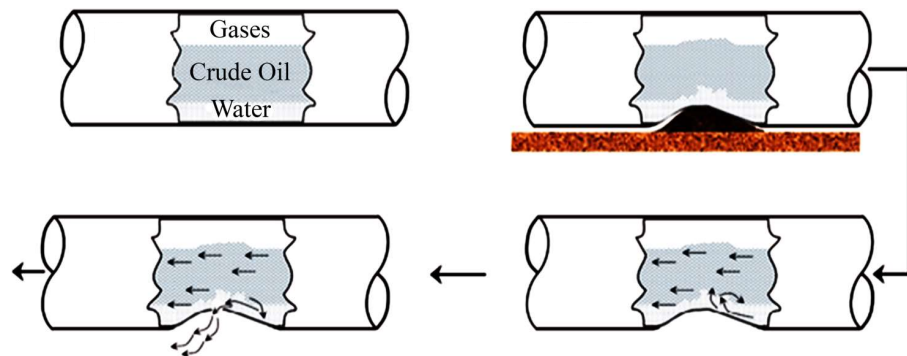

Fig. 9. Schematic illustration of a dent on pipe effect to the flow pattern inside

The hardness test depicts surface resistance due to material deformation through surface penetration and stretching methodology. The hardness value of the specimen of 80 HRB produces a microstructure comprised of ferrite and pearlite and indicates the diverse corrosion phenomenon [42]. In addition, the above microstructure phase accelerates the progress of corrosion, where the pearlite induces a faster speed of local corrosion [43]. The hardness test result also provides valuable information about active layer removal, which intensively protects the pipeline. This study proves that reducing the strength and rigidity of ex-spool material lowers their hardness.

The considerable hardness value also correlated to surface heterogeneity, confirming the reduction of carbon, phosphorus, manganese, and sulfur content.

The tensile test result also illustrates how the material has experienced plastic deformation. As exhibited in Table 4, the tensile strength of the specimen value is lower than the standard and refers to lower ductility and strength of materials. This value represents an approximately 2 % decrease in Ultimate Tensile Strength (UTS) and causes an increase in yield strength. At the same time, it lowers the mechanical properties and contributes to the noticeable rise in elongation after the tensile test.

The best explanation to describe the degradation of the materials is by capturing the linear relationship between the increase in corrosion rate and the gradual degradation of their mechanical properties. Based on the report of [44] provides clear guidance on the attacking process of electrolyte ions from seawater (which contains numerous ions) to the atomic structure of materials. It showcases that the internal surface of metals becomes less rigid and immediately reaches fatigue condition.

Notably, the root cause of failed ex-spool material remains related to the exfoliation of the thick corrosion film

in microstructure and their electrochemical reaction. Fig. 3 illustrates the condition of the microstructure of the ex-spool corroded area, and it shows the presence of the ferrite and pearlite (ferrite+cementite) phases.The work of [45] argues that the combination of ferritic and pearlitic MS structures exhibits remarkable mechanical properties compared to cast iron. However, the specimen of ex-spool 16'' MOL (comprised of ferrite and pearlite) likelihood of corrosion remains high due to the dissolution of metal under a high concentration of chloride ions in seawater.

It is believed that the white grains (Fig. 3) of ferrite are chemically active when the metal is exposed to brine to verify the transformation from α-iron to oxides and hydroxides of Fe^{2+} within the pearlite phase in the absence of cementite [46]. In the ferrite microstructure, the protective film's thickness was found. However, due to the abrasion of sand and high flow, the ferrite is eroded. In addition, the cementite lamellae of the pearlite grains provide the knowledge of the oxidation of ferrite Fe (in α-iron) into Fe^{2+}. The work [47] shows the dissolution of Fe^{2+} within the Fe_3C lamellar facilitates iron carbonate formation to promote the iron anodic dissolution.

On the other hand, the cementite acts as a cathodic region where the reduction occurs due to the low overvoltage of hydrogen [48]. The thin-film penetration of Fe^{2+} inside the inner layer allows the high content of Fe^{2+} and CO_3^{2-} which results in the supersaturation. It causes the precipitation of $FeCO_3$ and is responsible for local acidification since the resulting carbonic acid exists in a higher concentration of CO_2 gas and lowers the pH of the solution.

According to [49], the presence of Fe-cementite increases the pitting corrosion resistance of carbon steel by elevating the amount of Fe_3C. The pearlite is shown by the dark grains. There are no defects in terms of microstructure observed in the observed sample. The metallography result aligns with CO_2 harms the pearlitic carbon steel, as reported in the previous studies [50–52], and gives Fe_2CO_3 the predicted corrosion product. Both figures (Fig. 3) depict that ferrite inherent in a single-phase structure with the same morphology. Unlike ferrite, the pearlite shows a multiphase system corresponding to lamellar ferrite and Fe_3C.

The microstructure is observed to be expected for carbon steel. The metal loss observed results from continuous corrosion attack accompanied by corrosion product removal. As can be seen, the trace of remaining corrosion products is still observable in the microphotograph. Without proper mitigation, the anodic dissolution of iron might cause a more significant deterioration of the metal.

Fig. 4 shows the surface morphology of the failed material, and the presence of a flowery structure is evidence. The SEM microphotographs showed the crystal structure of iron oxides (cotton ball and flowery). Besides the structure of the cotton ball and flowery, irregular structures are also observed. The dominant element detected is iron, oxygen, chloride, and sulfur. As reported that the pipe was submerged in the sea, the chlorides could also be from the seawater ingress during lifting after pipe replacement.

Cracking on the surface of the metal is observed due to the volume expansion of the corrosion product. It can be observed from the SEM by 5000x magnification (Fig. 4, a, b). With increasing time exposure of the subsea pipeline in water, the small flowery floccule appears, which indicates the presence of α-FeOOH [52]. Furthermore, the SEM images could detect the goethite (cotton ball) associated with the increased localized corrosion due to the excessive amount of chloride (Table 5) [50] and agrees with the reported work [53]. It is suspected that the granular sand product existing on the coupon's surface of ex-spool material indicates the $γ-Fe_2O_3·H_2O$.

Based on Table 5, the amount of Fe and O dominates the composition of other compounds. The above result confirms iron carbonate and iron oxide are observed in the leak location. The growth of the damaged area correlates to the dent, which continually restricts fluid flow inwardly and causes the surrounding area to fail.

Results demonstrated that one common element in EDX is S, which proposed the organic components' microbial activity. The presence of sulfur in both locations shows a higher percentage of S (location 1) than in the second location. It shows the presence of FeS and the more S atom uptaken by the reaction between dissolved iron and S in this location.

Also, it shows the formation of oxides in the area of pearlitic[54] and confirms the examination of the preceding microstructure result. Table 5 shows that the total amount of the elements in location 1 is higher than in location 2, indicating a higher trace of corrosion product. The variation component in both areas corresponds to material corrosion resistance toward severe environmental conditions. The subsea location induces the threat of corrosion due to bacteria lowering the pH and yielding the organic acids. As a result, it breaks down the protected oxide layer.

In this work, it is predicted that microorganisms accept electrons and obtain the energy from the oxidation process of metal oxides when the shortage of energy from organic resources occurs [55]. The result confirmed the various corrosion products which were obtained using SEM. Therefore, a combination of all mentioned factors damages the condition of pipelines in the extended service run.

The compounds detected in the corrosion products collected from the internal pipe are shown in Fig. 5. It can be inferred that the depletion of S in the chemical composition is related to the formation of troilite, which is affected by the dissolved hydrogen sulfide gas (H_2S) in water. However, the higher displacement angle of FeS has not significantly influenced the failure of the specimen.

In contrast, the appearance of the siderite peak is in good agreement with the amount of dissolved CO_2 in water. The broadening of the siderite peaks at −0.014 indicates the inhomogenous surface from multiple corrosion products. It also correlatedto the scattered pit corrosion on the top of the coupon. The formation of hematite and magnetite is affected by the aqueous corrosion or weathering of the pipe material during outdoor exposure. Nevertheless, the small score of these compounds confirms that the presence of these compounds in the corrosion products was small. However, the analysis needs supporting data regarding the water analysis inside the pipeline. Therefore, the XRD results show that the CO_2 dominates the failure of failed material.

The result of seawater sampling activity to verify the contribution of sulfate-reducing bacteria (SRB) shows a gradual increment of bacteria's colony per milliliter of sample solution. It is a common practice that an alternative way to control the magnitude of bacteria is the addition of biocide. Equation (3) shows the complete reaction as previously studied by [56],

$$HCO_3^- + H^+ \rightarrow CO_2(g) + H_2O. \qquad (3)$$
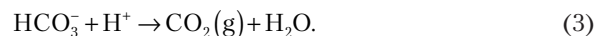
Equation (3) shows the high likelihood of the SRB producing CO_2. Therefore, the risk of uncontrolled SRB causing the excessive insoluble metal sulfide has been elucidated.

29

The work has explicitly introduced that the presence of CO_2 and bacterial activities have become a significant root cause of the failed material. From an industrial perspective and practice, pipeline inspection management (PIM) should align with RCA's evaluation to suggest a better maintenance program. Therefore, this paper bridges the RCA analysis and ILI Inspection. However, due to the high data volume of the inspection, it is challenging to learn the actual condition of pipelines using the conventional method. In this work, the implementation of PMM shows the great importance of using the ILI database to suggest the maintenance program of PIM.

The matrix calculates the correlation value between pairwise features in this work. It can be seen that the most related pairwise is shown by the PoF prediction and PoF-RuL. Hence, it justifies the argument of the equivalency between the PoF prediction and PoFRuL. By default, the prediction of failure can be summarized by calculating the remaining useful life, which projects the ratio between the thickness of inspected pipeline and the corrosion rate. This knowledge is adopted in this work to showcase the risk of corrosion due to CO_2 gas.

Fig. 7 shows that the pit corrosion length and width exhibit a low relationship with a score of 0.33. The relationship between the PoFRuL has a strong relationship (0.88) with PoF prediction and justifies the argument of the equivalency between the PoF prediction and PoFRuL. Moreover, the corrosion depth matches the PoFRuL as it has a score of 1. It shows that the corrosion depth has become the primary factor impacting materials'intergrity. The understanding agrees that the CO_2 corrosion increases the wall thinning of the inner layer of the pipeline. In the long run, it damages the pipeline and causes unprecedented shut-down.

On the other hand, the PoF prediction and the pipeline distance from the first pig launcher showed no correlation. It shows that the longer the pig launcher is from the initial position, the minimum effect of corrosion can be detected by the sensor device of ILI [57]. Also, there is a weak correlation between the width of the corrosion product and the PoF prediction (0.064).

In this work, the implementation of ML employs a few algorithms to project the correlation of all datasets provided by ILI inspection. RF, LR, and SVM are selected to predict whether the pipeline remains protected despite severely degraded a single section of its long pipeline. According to the result, the RF exhibits the highest impact with lower loss, indicating that nearly 1349 of the output data (the PoFRuL) are correctly predicted and represent the actual pipeline condition. The significance of RF shows its capability to collect decisions over numerous information on the decision tree, which is influenced by the input data and their model parameter [58]. On the contrary, the LR shows the lowest performance in suggesting the corrosion effect of CO_2 gas dissolution in water.

Based on the presented datasets, the most logical reasoning behind this value is the model merely approximates the probability of whether the pipelines become corrosive or non-corrosive. This dataset's LR is also unreliable since the model may not translate the non-linearity between the features and PoF prediction [59]. This result is similar to existing research [57] which emphasizes the weakness of LR due to a change of scales. Also, the LR is unreliable in translating the non-linearity between the features and PoF prediction in this dataset[58]. With this result, the accuracy of root-cause-analysis is significant and amplifies the human objectivity to assert the experimental judgment.

The limitation of the paper includes the types of material of API 581 X42 and the subsea environment. The failed material correlates to the peeled green coating in the inner layer of pipelines. However, the specification of the exfoliated coating requires extensive study. Moreover, the work remains to suffer to identify the type of bacteria progressively producing CO_2 gas. This uncertain classification may lead to improper corrosion mitigation and extends the more significant operational loss.

On the other hand, the utilization of Supervised Machine Learning to acquire knowledge from massive datasets is limited to Linear Regression (LR), Support Vector Machine (SVM), and Random Forest (RF) only. Unsupervised machine learning, such as Gaussian Mixture Models (GMM) [60], allows the engineer or scholar to predict the risk profile according to the risk's similarity. Pearson Multicollinear Matrix is used to evaluate the relationship between the parameter from the ILI data [61].

Pearson Multicollinear Matrix is used to evaluate the relationship between the parameter from the ILI data [61], despite the matrix only represents the correlation between the pairwise parameter. However, the improvement of risk distribution remains significant to achieving high prediction accuracy.

To this end, the disadvantage of this research covers the selection of characterization methods to elaborate the score of XRD compounds. The little score shows the amount of the corrosion product was lower in magnitude. Knowing the detailed information about the elemental composition increases the accuracy of the failed material inside the pipelines. Moreover, the principal causes of the failure remain unable to reveal the segmented risk of long pipelines. Due to the risk of corrosion being heterogeneous, the assumption of making generalization risk may not adequately affect inspection accuracy. As initially outlined, GMM is suitable for performing risk profiling and is the key to unlocking the actual condition of the corresponding pipeline under severe or non-severe conditions.

Therefore, the development of this research may be re-validated through comparison using several inspection data from various conditions and treatments. The validation of the ML model will appear to be adjusted due to different types of environments. Eventually, the approach to address the corrosion risk may vary due to conditions, temperatures, and environmental processes. Using the model, the engineer can quickly identify and evaluate the maintenance program, including adding a chemical inhibitor, cathodic protection, and another ILI inspection.

7. Conclusions

1. In this work, the depletion of Mn and dissolution of S composition suggest the ex-spool material fails due to its inadequacy to lower the speed effect of sand's erosion with the indication of the quantitative indicator. The result of visual inspection demonstrates that the severe corrosion location is at the 6 o'clock position. It is also possible to observe the exfoliated green internal coating and scratch lines to prove that the flow of sand abrasion appears. The pipeline's dent further slowers the fluid flow velocity and is accountable for the pipeline's strength reduction. In addition, the elongation has risen at 33 %, confirming the movement of the atomic structure generated from intensive moving

abrasive substances to provide a more extensive deposition of corrosion product.

2. The appearance of siderite (displacement angle of −0.014) confirmsthe presence of the ferrite and pearlite phases. The results demonstrate that the CO_2 gas is responsible for the failure material. The white grains of ferrite remain observed on the surface of an ex-spool specimen, which is associated with α-Iron transformation to Fe-oxide and hydroxide. The pearlite of black grains corresponds with a combination between ferrite and cementite. The appearance of two phases is evident in the SEM image and reflected in the percentage composition of EDX as corrosion products. Furthermore, cracking appears due to a greater volume of corrosion product where the α-FeOOH and γ-Fe_2O_3·H_2O represent the flowery and cotton ball structures.

3. Bacterial activity lowers the material's mechanical properties with qualitative indication. The microorganism continuously produces the CO_2 gas, which is attractive to dissolve Fe^{2+} to give $FeCO_3$ and reduce surface passivation against corrosion.

4. The PMM shows the strongest correlation between corrosion depth and the PoF prediction, which provides the highest score of 0.88. The sole parameter of wall thinning due to CO_2 corrosion from the modeling method agrees with the experimental result with the indication of qualitative and quantitative from the research development. In addition, RF provides the best model to demonstrate the risk of corrosion with 92.18 % accuracy. At the same time, LR shows thatitmay be insufficient to map the relationship between the label and features data (67.81 %). The two algorithms correctly compare the indication of corrosion, both quantitative and qualitative.

References

1. Gao, J., Yang, P., Li, X., Zhou, J., Liu, J. (2019). Analytical prediction of failure pressure for pipeline with long corrosion defect. Ocean Engineering, 191, 106497.doi: https://doi.org/10.1016/j.oceaneng.2019.106497

2. Aalirezaei, A., Kabir, G. (2021). A bibliometric analysis on oil and gas pipeline failure consequence analysis.Innovative Infrastructure Solutions, 6 (4).doi: https://doi.org/10.1007/s41062-021-00591-0

3. Zakikhani, K., Nasiri, F., Zayed, T. (2020). A Review of Failure Prediction Models for Oil and Gas Pipelines. Journal of Pipeline Systems Engineering and Practice, 11 (1).doi: https://doi.org/10.1061/(asce)ps.1949-1204.0000407

4. Aljaroudi, A., Khan, F., Akinturk, A., Haddara, M., Thodi, P. (2015). Risk assessment of offshore crude oil pipeline failure. Journal of Loss Prevention in the Process Industries, 37, 101–109. doi: https://doi.org/10.1016/j.jlp.2015.07.004

5. Rachman, A., Zhang, T., Ratnayake, R. M. C. (2021). Applications of machine learning in pipeline integrity management: A state-of-the-art review. International Journal of Pressure Vessels and Piping, 193, 104471.doi: https://doi.org/10.1016/j.ijpvp.2021.104471

6. Aditiyawarman, T., Kaban, A. P. S., Soedarsono, J. W. (2022). A Recent Review of Risk-Based Inspection Development to Support Service Excellence in the Oil and Gas Industry: An Artificial Intelligence Perspective. ASCE-ASME J Risk and Uncert in Engrg Sys Part B MechEngrg, 9 (1).doi: https://doi.org/10.1115/1.4054558

7. Alsahli, M. S., Almasri, M. M., Al-Akhras, M., Al-Issa, A. I., Alawairdhi, M. (2021). Evaluation of Machine Learning Algorithms for Intrusion Detection System in WSN.International Journal of Advanced Computer Science and Applications, 12 (5).doi: https://doi.org/10.14569/ijacsa.2021.0120574

8. Paul Setiawan Kaban, A., Mayangsari, W., Syaiful Anwar, M., Maksum, A., Riastuti, R., Aditiyawarman, T., Wahyuadi Soedarsono, J. (2022).Experimental and modelling waste rice husk ash as a novel green corrosion inhibitor under acidic environment. Materials Today: Proceedings, 62, 4225–4234. doi: https://doi.org/10.1016/j.matpr.2022.04.738

9. Kaban, A. P. S., Ridhova, A., Priyotomo, G., Elya, B., Maksum, A., Sadeli, Y. et. al. (2021). Development of white tea extract as green corrosion inhibitor in mild steel under 1 M hydrochloric acid solution. Eastern-European Journal of Enterprise Technologies, 2 (6 (110)), 6–20. doi: https://doi.org/10.15587/1729-4061.2021.224435

10. Kaban, E. E., Maksum, A., Permana, S., Soedarsono, J. W. (2018). Utilization of secang heartwood (caesalpiniasappan l) as a green corrosion inhibitor on carbon steel (API 5L Gr. B) in 3.5% NaCl environment. IOP Conference Series: Earth and Environmental Science, 105, 012062. doi: https://doi.org/10.1088/1755-1315/105/1/012062

11. Azmi, M. F., Soedarsono, J. W. (2018). Study of corrosion resistrance of pipeline API 5L X42 using green inhibitor bawangdayak (EleutherineamericannaMerr.) in 1M HCl. IOP Conference Series: Earth and Environmental Science, 105, 012061. doi: https://doi.org/10.1088/1755-1315/105/1/012061

12. Leuvinadrie, L. P., Soedarsono, J. W. M. (2021). Pipe stress simulation and failure analysis of carbon steel flange spool in CO_2 gas flow condition. PROCEEDINGS OF THE 13TH AUN/SEED-NET REGIONAL CONFERENCE ON MATERIALS (RCM 2020) AND THE 1ST INTERNATIONAL CONFERENCE ON MATERIALS ENGINEERING AND MANUFACTURING (ICMEM 2020). doi: https://doi.org/10.1063/5.0070886

13. Bahrami, A., Khouzani, M. K., Harchegani, B. B. (2021).Establishing the root cause of a failure in a firewater pipeline.Engineering Failure Analysis, 127, 105474.doi: https://doi.org/10.1016/j.engfailanal.2021.105474

14. Gong, Y., Du, M.-Y., Ma, F.-Q., He, G.-Q., Xue, Y., Jiao, C.-S. et. al. (2020). Failure analysis and prevention of corrosion occurring during storage on steam generator tube sheet for advanced PWR, Part I: Root causes analysis. Engineering Failure Analysis, 116, 104710. doi: https://doi.org/10.1016/j.engfailanal.2020.104710

15. Yang, Y., Khan, F., Thodi, P., Abbassi, R. (2017). Corrosion induced failure analysis of subsea pipelines. Reliability Engineering & System Safety, 159, 214–222. doi: https://doi.org/10.1016/j.ress.2016.11.014

16. Lopez, M. et. al. (2015). Internal corrosion solution for gathering production gas pipelines involving palm oil amide based corrosion inhibitors. Int. J. Electrochem. Sci., 10, 7166–7179. Available at: http://www.electrochemsci.org/papers/vol10/100907166.pdf

17. Khera, A., Baniah, B. B. (2017). Internal Corrosion Predicted and Found in Refined Piggable Product Pipeline Through ICDA. ASME 2017 India Oil and Gas Pipeline Conference.doi: https://doi.org/10.1115/iogpc2017-2449

18. Melo, C., Dann, M. R., Hugo, R. J., Janeta, A. (2020). Optimal locations for non-destructive inspections to verify direct assessment of internally corroded pipelines.Upstream Oil and Gas Technology, 5, 100008.doi: https://doi.org/10.1016/j.upstre.2020.100008

19. Zapevalov, D. N., Vagapov, R. K. (2021). Analysis of regulatory requirements for the assessment of carbon dioxide corrosion at gas production facilities. Issues of Risk Analysis, 18 (2), 60–71. doi: https://doi.org/10.32686/1812-5220-2021-18-2-60-71

20. Wolodko, J., Alemaskin, K., Adane, K. F., Jaimes, V., Lipsett, M. (2019). Development of a novel testing method for characterizing wet sliding abrasion in slurry transport systems.CORROSION 2019. Available at: https://onepetro.org/NACECORR/proceedings-abstract/CORR19/All-CORR19/NACE-2019-13458/127440

21. Daniyan, I., Balogun, V., Ererughurie, O. K., Daniyan, L., Oladapo, B. I. (2021). Development of an inline inspection robot for the detection of pipeline defects. Journal of Facilities Management, 20 (2), 193–217. doi: https://doi.org/10.1108/jfm-01-2021-0010

22. Rachman, A., Ratnayake, R. M. C. (2019). Machine learning approach for risk-based inspection screening assessment. Reliability Engineering & System Safety, 185, 518–532. doi: https://doi.org/10.1016/j.ress.2019.02.008

23. Xie, M., Sutherland, J., Fang, B., Gu, B., Tian, Z. (2020). Impact Analysis of Inline Inspection Accuracy on Pipeline Integrity Planning.Journal of Pressure Vessel Technology, 142 (6).doi: https://doi.org/10.1115/1.4047270

24. DNV-RP-F101. Corroded Pipelines.

25. DNV. Risk Based Inspection of Offshore Topsides Static Mechanical Equipment.

26. Kuhn, M., Johnson, K. (2013). Applied predictive modeling.Springer, 600.doi: https://doi.org/10.1007/978-1-4614-6849-3

27. Zhang, C., Liu, C., Zhang, X., Almpanidis, G. (2017). An up-to-date comparison of state-of-the-art classification algorithms. Expert Systems with Applications, 82, 128–150. doi: https://doi.org/10.1016/j.eswa.2017.04.003

28. Brown, I., Mues, C. (2012). An experimental comparison of classification algorithms for imbalanced credit scoring data sets. Expert Systems with Applications, 39 (3), 3446–3453. doi: https://doi.org/10.1016/j.eswa.2011.09.033

29. Rodriguez-Galiano, V. F., Ghimire, B., Rogan, J., Chica-Olmo, M., Rigol-Sanchez, J. P. (2012). An assessment of the effectiveness of a random forest classifier for land-cover classification. ISPRS Journal of Photogrammetry and Remote Sensing, 67, 93–104. doi: https://doi.org/10.1016/j.isprsjprs.2011.11.002

30. Furey, T. S., Cristianini, N., Duffy, N., Bednarski, D. W., Schummer, M., Haussler, D. (2000). Support vector machine classification and validation of cancer tissue samples using microarray expression data. Bioinformatics, 16 (10), 906–914. doi: https://doi.org/10.1093/bioinformatics/16.10.906

31. Hao, X., Zhao, X., Chen, H., Huang, B., Ma, J., Wang, C., Yang, Y. (2021). Comparative study on corrosion behaviors of ferrite-pearlite steel with dual-phase steel in the simulated bottom plate environment of cargo oil tanks. Journal of Materials Research and Technology, 12, 399–411. doi: https://doi.org/10.1016/j.jmrt.2021.02.095

32. Li, J., Du, C., Liu, Z., Li, X. (2022). Extracellular electron transfer routes in microbiologically influenced corrosion of X80 steel by Bacillus licheniformis.Bioelectrochemistry, 145, 108074.doi: https://doi.org/10.1016/j.bioelechem.2022.108074

33. King, R. A., Miller, J. D. A., Smith, J. S. (1973). Corrosion of Mild Steel by Iron Sulphides. British Corrosion Journal, 8 (3), 137–141. doi: https://doi.org/10.1179/000705973798322251

34. Li, Y., Feng, S., Liu, H., Tian, X., Xia, Y., Li, M. et. al. (2020). Bacterial distribution in SRB biofilm affects MIC pitting of carbon steel studied using FIB-SEM. Corrosion Science, 167, 108512. doi: https://doi.org/10.1016/j.corsci.2020.108512

35. Xie, M., Tian, Z. (2018). A review on pipeline integrity management utilizing in-line inspection data.Engineering Failure Analysis, 92, 222–239.doi: https://doi.org/10.1016/j.engfailanal.2018.05.010

36. Inman, S., Han, J., Gerard, A., Qi, J., Wischhusen, M., Agnew, S. et. al. (2021).Effect of Mn Content on the Passivation and Corrosion of $Al_{0.3}Cr_{0.5}Fe_2Mn_xMo_{0.15}Ni_{1.5}Ti_{0.3}$ Compositionally Complex Face-Centered Cubic Alloys. Corrosion, 78 (1), 32–48. doi: https://doi.org/10.5006/3906

37. Raj, P. N., Raha, B., Sekar, K., Joseph, M. (2021). Effect of Manganese on Synergistic Erosion–Corrosion Characteristics of A890 7A Hyper Duplex Stainless Steels.Journal of Materials Engineering and Performance, 31 (1), 11–23.doi: https://doi.org/10.1007/s11665-021-06148-7

38. Mondal, K., Sathithsuksanoh, N., Lalvani, S. B. (2020). Electrodeposition and characterization of NiCoP. SN Applied Sciences, 2 (12). doi: https://doi.org/10.1007/s42452-020-03921-6

39. Jiang, Z., Guoyong, L., Yuan, Y., Youdong, J., Xue, G. (2020). Improving sulfur corrosion resistance of transformer windings by grain boundary engineering technology. IEEE Transactions on Dielectrics and Electrical Insulation, 27 (3), 1022–1028. doi: https://doi.org/10.1109/tdei.2020.008735

40. Cui, L., Kang, W., You, H., Cheng, J., Li, Z. (2020). Experimental Study on Corrosion of J55 Casing Steel and N80 Tubing Steel in High Pressure and High Temperature Solution Containing CO_2 and NaCl. Journal of Bio- and Tribo-Corrosion, 7 (1). doi: https://doi.org/10.1007/s40735-020-00449-5

41. Javidi, M., Bekhrad, S. (2018). Failure analysis of a wet gas pipeline due to localised CO_2 corrosion. Engineering Failure Analysis, 89, 46–56.doi: https://doi.org/10.1016/j.engfailanal.2018.03.006

42. Liu, H., Wei, J., Dong, J., Chen, Y., Wu, Y., Zhou, Y. et. al. (2021). Influence of cementite spheroidization on relieving the micro-galvanic effect of ferrite-pearlite steel in acidic chloride environment. Journal of Materials Science & Technology, 61, 234–246. doi: https://doi.org/10.1016/j.jmst.2020.05.031

43. Wang, Z., Zhang, X., Cheng, L., Liu, J., Wu, K. (2021). Role of inclusion and microstructure on corrosion initiation and propagation of weathering steels in marine environment. Journal of Materials Research and Technology, 10, 306–321. doi: https://doi.org/10.1016/j.jmrt.2020.11.096

44. Hamidah, I., Solehudin, A., Hamdani, A., Hasanah, L., Khairurrijal, K., Kurniawan, T. et. al. (2021).Corrosion of copper alloys in KOH, NaOH, NaCl, and HCl electrolyte solutions and its impact to the mechanical properties. Alexandria Engineering Journal, 60 (2), 2235–2243. doi: https://doi.org/10.1016/j.aej.2020.12.027

45. Dwivedi, D., Rowles, M. R., Becker, T., Lepkova, K. (2020). The role of ferrite-cementite interface in formation of hierarchical film on carbon steel in CO_2-saturated brine. Applied Surface Science, 509, 145107.doi: https://doi.org/10.1016/j.apsusc.2019.145107

46. Yang, Y., Fan, X., Casillas, G., Peng, Z., Ruan, G., Wang, G. et. al. (2014).Three-Dimensional Nanoporous Fe_2O_3/Fe_3C-Graphene Heterogeneous Thin Films for Lithium-Ion Batteries. ACS Nano, 8 (4), 3939–3946. doi: https://doi.org/10.1021/nn500865d

47. Sun, J. B., Zhang, G. A., Liu, W., Lu, M. X. (2012). The formation mechanism of corrosion scale and electrochemical characteristic of low alloy steel in carbon dioxide-saturated solution. Corrosion Science, 57, 131–138. doi: https://doi.org/10.1016/j.corsci.2011.12.025

48. López, D., Schreiner, W., de Sánchez, S., Simison, S. (2003). The influence of carbon steel microstructure on corrosion layers. Applied Surface Science, 207 (1-4), 69–85. doi: https://doi.org/10.1016/s0169-4332(02)01218-7

49. Syugaev, A. V., Lomaeva, S. F., Reshetnikov, S. M., Shuravin, A. S., Sharafeeva, E. F., Surnin, D. V. (2008). The effect of the structure-phase state of iron-cementite nanocomposites on local activation processes. Protection of Metals, 44 (4), 367–371. doi: https://doi.org/10.1134/s0033173208040097

50. Masoumi, M., Béreš, M., Herculano, L. F. G., de CarvalhoPaesLoureiro, R., de Abreu, H. F. G. (2020). Microstructure and Crystallographic Texture Changes under Torsion Loading of Pearlitic Steel Strips.Journal of Materials Engineering and Performance, 29 (11), 7250–7259.doi: https://doi.org/10.1007/s11665-020-05232-8

51. De CarvalhoPaesLoureiro, R., Beres, M., Masoumi, M., Ferreira Gomes de Abreu, H. (2021). The effect of pearlite morphology and crystallographic texture on environmentally assisted cracking failure. Engineering Failure Analysis, 126, 105450.doi: https://doi.org/10.1016/j.engfailanal.2021.105450

52. Yuan, Y., Liu, X., Pu, G., Wang, T., Zheng, D. (2021). Temporal and spatial variability of corrosion of high-strength steel wires within a bridge stay cable. Construction and Building Materials, 308, 125108.doi: https://doi.org/10.1016/j.conbuildmat.2021.125108

53. Antunes, R. A., Costa, I., Faria, D. L. A. de. (2003). Characterization of corrosion products formed on steels in the first months of atmospheric exposure. Materials Research, 6 (3), 403–408. doi: https://doi.org/10.1590/s1516-14392003000300015

54. Kim, B. H., Kim, H., Hyun, M. S., Park, D. H. (1999). Direct electrode reaction of Fe(III)-reducing bacterium, Shewanellaputrefaciens. Journal of Microbiology and Biotechnology, 9, 127–131.

55. Xu, Y.-N., Chen, Y. (2020). Advances in heavy metal removal by sulfate-reducing bacteria. Water Science and Technology, 81 (9), 1797–1827. doi: https://doi.org/10.2166/wst.2020.227

56. Kraus, M., Feuerriegel, S. (2019). Forecasting remaining useful life: Interpretable deep learning approach via variational Bayesian inferences. Decision Support Systems, 125, 113100. doi: https://doi.org/10.1016/j.dss.2019.113100

57. Han, Q., Gui, C., Xu, J., Lacidogna, G. (2019). A generalized method to predict the compressive strength of high-performance concrete by improved random forest algorithm. Construction and Building Materials, 226, 734–742. doi: https://doi.org/10.1016/j.conbuildmat.2019.07.315

58. Rijnhart, J. J. M., Twisk, J. W. R., Eekhout, I., Heymans, M. W. (2019). Comparison of logistic-regression based methods for simple mediation analysis with a dichotomous outcome variable. BMC Medical Research Methodology, 19 (1).doi: https://doi.org/10.1186/s12874-018-0654-z

59. Ahmed, I. A. I., Cheng, W. (2020). The Performance of Robust Methods in Logistic Regression Model. Open Journal of Statistics, 10 (01), 127–138. doi: https://doi.org/10.4236/ojs.2020.101010

60. Löffler, M., Zhang, A. Y., Zhou, H. H. (2021). Optimality of spectral clustering in the Gaussian mixture model.The Annals of Statistics, 49 (5).doi: https://doi.org/10.1214/20-aos2044

61. Hasnain, M., Pasha, M. F., Ghani, I., Imran, M., Alzahrani, M. Y., Budiarto, R. (2020). Evaluating Trust Prediction and Confusion Matrix Measures for Web Services Ranking. IEEE Access, 8, 90847–90861. doi: https://doi.org/10.1109/access.2020.2994222